Appl. Phys. B 61, 325–332 (1995)

Applied Physics B Lasers and Optics

Layout and performance of the Asterix IV iodine laser at MPQ, Garching

H. Baumhacker, G. Brederlow, E. Fill, R. Volk, S. Witkowski, K.J. Witte

Max-Planck-Institut für Quantenoptik (MPQ), Hans-Kopfermann-Strasse 1, D-85740 Garching, Germany
(Fax: + 49-89/32905-200)

Received: 3 April 1995/Accepted: 30 May 1995

Abstract. In this paper, the design procedure and the performance of the single beam Asterix IV high-power iodine laser emitting at $\lambda = 1315$ nm is described. It has been developed on the basis of a 10-years experience with the 1 TW Asterix III laser-system and with the support of a 1-D and a 3-D pulse propagation code. Special emphasis has been put on achieving a high overall system efficiency and a beam intensity profile as homogeneous as possible. Presently, Asterix IV provides output pulses with durations from 0.2 to several ns. At a duration of 0.4 ns, the pulse power is 3 TW and at a duration of 5 ns the pulse energy reaches 2.1 kJ. Under these conditions, the laser can be fired every twenty minutes.

PACS: 42.55.Lt; 42.60.Jf; 52.80.Mg

1 Method of excitation and basic medium properties

The high-power potential of the iodine laser was first demonstrated at MPQ, Garching [1]. This laser type is capable of delivering multi-kilojoule pulses with durations around 1 ns at a nearly diffraction-limited beam quality. The laser medium is a mixture of a gaseous alkyliodide and a buffer gas, usually C_3F_7I and argon. The alkyliodide is photodissociated by UV-pump light in the wavelength region from 240 to 320 nm yielding the radical C_3F_7 and an excited iodine atom in the upper laser level $^2P_{12}$. The lower one corresponds to the ground state of the iodine atom $^2P_{3/2}$. The transition is of the magnetic dipole type and occurs at a wavelength of $\lambda = 1315$ nm [2].

Among the various methods of excitation [2] only two have gained practical importance. One is based on laser pumping by surface discharges or wire explosions embedded in the laser medium (pump time: 35–50 μs) and the other on fast flashlamp pumping (pumping time: 10 μs region) [3–5]. The first concept is technologically less demanding. The second one has the advantage that due to the shorter pumping time the laser medium shows a better optical homogeneity and disadvantageous effects resulting from the laser kinetics, e.g., quenching, are reduced. Moreover, higher shot rates can be realized with the second concept. For the Asterix laser external flashlamp pumping has thus been employed.

The iodine laser is less subject to problems of optical damage by self-focusing effects than solid-state high-power lasers and provides a greater flexibility in choosing the most suitable operating conditions. This is due to the fact that the stimulated emission cross section of the laser transition can easily be adjusted to its optimal value by pressure broadening through a buffer gas [2]. In addition, the value of the saturation energy density of about $1 J/cm^2$ is very favorable for efficient single-pass energy extraction out of an amplifier.

2 Layout of Asterix IV

At first the 300 J/1 TW Asterix III laser was built and applied for laser plasma experiments until 1985 [5]. Since 1989 these investigations and additional X-ray laser experiments have been carried out with Asterix IV. This laser is a completely new design, based on the know-how gained with Asterix III and on the support of a well-proven 1-D pulse propagation code developed at MPQ [6]. It was used to optimize the amplifier chain concerning extraction efficiency and to follow the pulse shortening caused by saturation in amplifier and absorbers. This latter information is helpful in two respects. Firstly, it eases the identification of possible damage sites in the chain due to too high a beam loading resulting from pulse compression. Secondly, it reveals how sensitively the output pulse duration is correlated to the input pulse duration under various operating conditions. This knowledge is important for laser plasma experiments where the pulse duration is a critical issue.

Our main goals in constructing Asterix IV was to get more energy than Asterix III at a better overall efficiency and a beam profile being as close as possible to a top hat.

Therefore, a new amplifier layout and a beam guiding system comprising image relaying combined with spatial filtering was introduced. The laser was projected to deliver an output energy of up to 2 kJ ($t_p \geq 1$ ns) and a maximum power of 5 TW ($t_p \leq 0.2$ ns) at output pulse lengths ranging from 0.2 to 5 ns.

2.1 Overall system

The scheme of Asterix IV is shown in Fig. 1. An acousto-optically mode-locked oscillator and a long-pulse oscillator provide a sufficient output width variability. The acousto-optically mode-locked oscillator delivers a train of about 10 pulses with essentially equal properties. By changing the medium bandwidth and the acoustic power fed into the mode coupler the pulse duration can be varied from 0.3–1.0 ns. The long-pulse oscillator generates a smooth pulse without any substructure whose width can be chosen between 3 and 15 ns by changing the resonator length. Both a one-way ring resonator and an actively stabilized Fabry-Perot cavity have been proven to be equally well suited. The short-pulse generation mechanism is due to ultrafast gain switching achieved by pumping the alkyliodide, C_2F_5I in this case, by a 15 ns long KrF-laser pulse [7]. With the pulses of these two oscillators the duration of the pulses leaving the chain can be varied between 0.2 and 0.7 ns when the mode-locked oscillator is used and between 1 and 5 ns in the case of the gain-switched oscillator. The reduction in pulse duration is due to saturation effects in the amplifiers and the absorber.

From the pulse train delivered from the mode locked oscillator a specially developed pulse selection system selects one pulse for further amplification [8]. The characteristic feature of this system is that the energy of the pulse which precedes the transmitted one and switches the laser-triggered spark gap is beforehand enhanced to the 10 mJ level in the first amplifier. Thus, a high reliability (system failure rate: $< 0.1\%$) and a low jitter (± 0.3 ns) could be achieved. With the laser-triggered spark gap not only the two Pockels cells of the pulse selection system and the cell behind the first amplifier (extinction ratio of each: $1:10^3$) but also those located behind the second and third amplifiers (extinction ratio of each: 1:200) are switched (Fig. 1). Thus, a high prepulse suppression could be obtained. In the gain-switched oscillator the single pulse emitted is split into two pulses. One serves for switching the laser-triggered spark gap and the other for seeding the amplifier chain.

This chain consists of six amplifiers of increasing diameter and length. The layout of these amplifiers is such that the input energy density is in the region of the saturation energy density (≈ -0.9 J/cm^2) and the output energy density does into exceed 3J/cm^2. Thus, an extraction efficiency for the stored inversion energy between 50 and 55% is obtained. All the amplifiers are assembled from modules, which contain the quartz tube for the gaseous laser medium and the surrounding flashlamps with their reflectors. Flashlamps and reflectors are mounted on plastic half shells for easy maintenance. To achieve saturation already in the third amplifier, the second is operated in the double pass mode. The incoming and outgoing beams are separated by a polarizer, whereby the polarization plane is rotated by passing a quarter-wave plate twice. The last amplifier consists of eight sections. It has an active length of 8 m and an effective aperture of 29 cm and is equipped with 96 flashlamps.

To maintain an optimal filling factor for the pulse at high loading a rectangular and smooth intensity profile has to be generated. Since an initially smooth intensity profile will be distorted by diffraction effects, image relaying has to be applied. For this purpose the image of a homogeneously illuminated aperture with a clear diameter of 8 mm positioned at the entrance of the first telescope is successively imaged through the amplifier

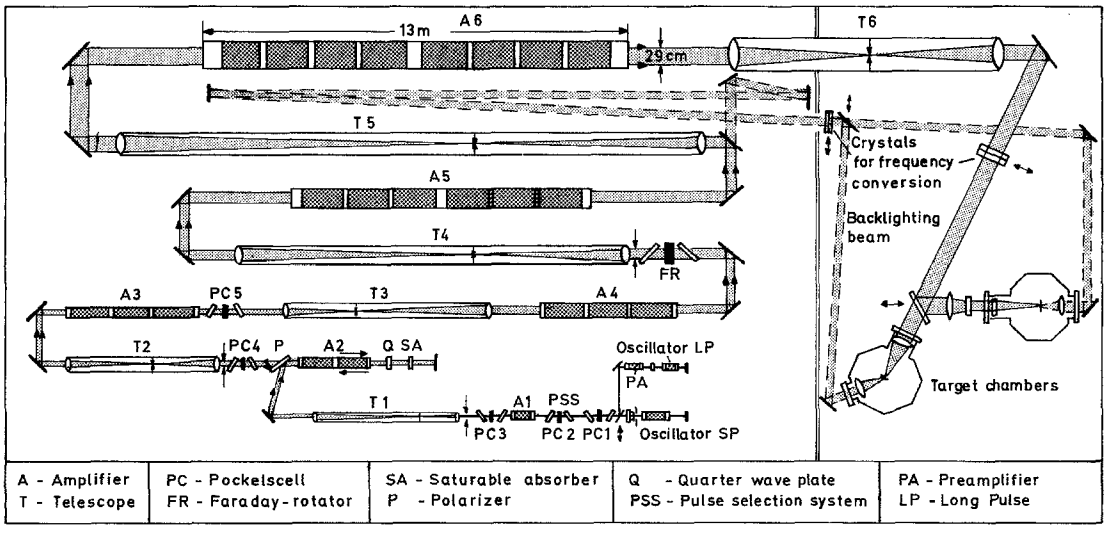

Fig. 1. Scheme of the Asterix IV laser

chain from one amplifier exit to the next. The telescopes of this system also serve for beam expansion and spatial filtering. This filtering performed by apertures with 10 times diffraction-limited diameters is required to remove the high spatial frequency components from the angular beam spectrum which may arise from medium inhomogeneities, diffraction, and self-focusing effects. The latter mainly occur in the glass windows of the amplifiers at pulse lengths $t_p < 0.7$ ns since the nonlinear index of refraction of glass has 10^3 times the value of that of the gaseous laser medium. Spatial filtering provides also amplifier decoupling to some degree.

Due to the slightly concave inversion density profile in the first amplifiers and amplification in the saturation regime [9] the beam intensity profile shows an edge enhancement. This is, however, suppressed by a soft aperture placed at the exit of the fourth amplifier. Such dielectrically coated soft apertures have been developed at MPQ [10]. They exhibit a soft transition of the transmission $\geq 95\%$ at the center part to about 10% at the edges. Shape and dimensions of the transmission zone can be chosen as free parameters.

A saturable absorber and several Pockells cells serve for mirror- and amplifier decoupling and for prepulse reduction. Even at 1 ω only one Faraday rotator is necessary to protect the laser system from light retro-reflected from the target. This is due to the small bandwidth of the iodine transition of less than 1 cm^{-1} and a frequency shift of the back-reflected light.

The laser pulse can be frequency doubled or tripled by using two KD*P type II crystals mounted in a common case in the polarization mismatch scheme as suggested by Craxton [11]. Their thicknesses of 15 and 13 mm, respectively, are optimized for a power density of 3 GW/cm^2. The crystals are positioned in the image plane of the last telescope.

For the laser-plasma and X-ray laser experiments an auxiliary beam was installed. Its timing can be varied in the region between some nanoseconds ahead and some after the main pulse. The pulse energy is adjustable in the range of up to 20% of the main pulse energy. The laser light of the auxiliary pulse can also be converted by KD*P crystals into the second and third harmonic.

The laser system with a multiply folded total beam path length of 175 m is mounted on a 70 cm thick concrete plate mechanically decoupled from the building. It is located in a temperature ($\pm$ 1°C) and humidity ($\leq 70\%$) stabilized clean-room 15×30 m^2 in size and of the clean-room class 10^3 to 10^4. The alignment of the laser beam is performed semi-automatically using a cw YAG laser at $\lambda = 1319$ nm and infrared sensitive vidicons.

2.2 Laser-medium handling and replacement

After a shot, the photo-dissociated C_3F_7I molecules do not completely recombine and strongly quenching photolytic products such as I_2 appear. To replace the dissociated laser medium ($\approx 5\%$) and to remove the quenching components, an automatic laser-medium regeneration system is installed. In this system liquid C_3F_7I is stored at such a temperature ($-60 \leq T \leq -20$°C) that its vapour pressure corresponds to the pressure required in the amplifier. Depending on the size of the amplifier this temperature ranges from -12 to -60°C whereby the smaller amplifiers require the lower temperatures. After a shot, the laser medium circulates through the cooled storage vessel. The quenching products then condensate and the used-up portion of the laser medium is replaced by an equivalent amount of freshly vaporized C_3F_7I. This sealed-off regeneration system has to be exchanged after 3 to 24 months, whereby the longer periods hold for the smaller amplifiers. The partial pressure p of the C_3F_7I determines the radial inversion density profile in the amplifiers and hence the intensity profile of the laser beam. In amplifiers with a diameter d, a rectangular profile will be obtained when the relation $p\,d = 200$ mbar cm is satisfied. The regeneration system will keep p within the limits of $\pm$ 3% of the required value. For the last three amplifiers the actual value of p is monitored by an UV-light absorption method.

The shot rate of the laser system depends mainly on the replacement time of the portion of the used-up laser medium and, since the laser beam shows a downward deflection after a shot, also on the recovery time of the original laser beam direction.

To ensure a faster laser-medium replacement the stored liquid C_3F_7I is locally and temporarily heated for the last three amplifiers. Thus, the required partial pressure can be restored within 10 min.

The downward deflection of the laser beam is due to the fact that laser gas heated by the flashlamp radiation accumulates in the upper part of the laser tube. Thus, a vertical temperature gradient arises leading to a vertical refractive index gradient. To reduce this effect, the laser medium, flowing in a closed loop through the amplifiers and the regeneration systems after each shot, is forced to pass the amplifiers in a helicoidal manner. Thus, the directional stability could be reestablished within 10 min. In addition, the heat released by the flashlamps is cooled off by a closed nitrogen loop.

With the recently improved regeneration and flow-guiding systems the shot rate was raised from one shot per hour to now one shot every 20 min. If necessary, it can be further enhanced by supplying the storage vessels of the regeneration systems of the first three amplifiers with heating elements.

2.3 Flashlamps

The Asterix IV laser is pumped by 172 flashlamps of different sizes and loadings. The flashlamps were developed at MPQ because commercial sealed lamps show an about 20% reduction of the pumping efficiency at the required high loading after 20–30 shots. This is due to a release of molecular impurities which prevent the electrons from reaching their optimal temperature. The MPQ flashlamps, therefore, allow for an exchange of the Xe gas. The largest lamps are those of the last three amplifiers. They have a maximum active length of 95 cm at an inner diameter of 2.5 cm. Their maximum loading is 8 kJ at 40 kV (explosion limit: ≈ 20 kJ). The discharge circuit is nearly critically damped with a half-cycle discharge time

of 20 μs. These lamps are equipped with elliptic reflectors such that one of its foci coincides with or is at least close to the discharge channel in the flashlamp and the other with the center of the amplifier tube. Computations with a ray-tracing code revealed that the homogeneity of the inversion profile sensitively depends on the coincidence of the discharge channel with the reflector focus position (Fig. 2). For the case that the discharge channel and the focus position deviate, the inversion density does not reach its optimal value in the center of the amplifier and hot spots are formed. Since, however, this coincidence is difficult to achieve, the imaging properties of the reflectors have been blurred by a soft sandblasting of their surfaces.

When the reflector serves as a current return path, streak camera pictures show, that the current always flows on that wall side which is closest to the reflector. This is due to the fact that, before ignition, the electric field strength is highest in the gap between the high-voltage electrode (anode) and the grounded reflector. Therefore, the electric breakdown occurs in this direction along the reflector wall side. The current then stays in this location since the transverse $j \times B$ forces are not strong enough to blow the discharge towards the axis of the lamp. Thus, the wall loading is highest on this side and cracks will develop which lead to a weakening of the wall structure. The flashlamps have therefore to be exchanged after 250–350 shots. If, however, the electric field before ignition is always axially symmetric breakdown will take place along the flashlamp axis. This situation is realized in a configuration shown in Fig. 3. The current flows here in four wires surrounding the lamp symmetrically. The floating reflector now only serves for the coupling of the pumping light into the amplifier. With this arrangement, the lifetime of the flashlamps increases almost by a factor of three. The lamps have then to be replaced after 750–1000 shots. Additionally, an increase of the pumping efficiency by about 10% could be observed.

2.4 Diagnostics

For supervising the laser performance, a diagonostic system is installed which provides information on both the technical status of the main components of the installation and the pulse properties. Concerning the technical status the following quantities are measured: charging voltages of the capacitor banks, amplitude and time behaviour of the UV-light emission of the flashlamps, temperatures in various positions of the laser-medium circulation and flashlamp cooling systems, alkyliodide and total pressures in each amplifier. Concerning the pulse properties the following measurements are taken: location of the selected pulse in the oscillator pulse train and its position in the gate of the pulse selection system, input and output energies for each amplifier, prepulse energy at the exit of the last amplifier, pulse durations behind the first and the final amplifier, beam energy density profile in a plane equivalent to that of the frequency conversion crystals, and beam focusability. Moreover, if required, possible parasitic oscillations in the amplifier chain can be monitored. Most of these data are automatically recorded after each shot.

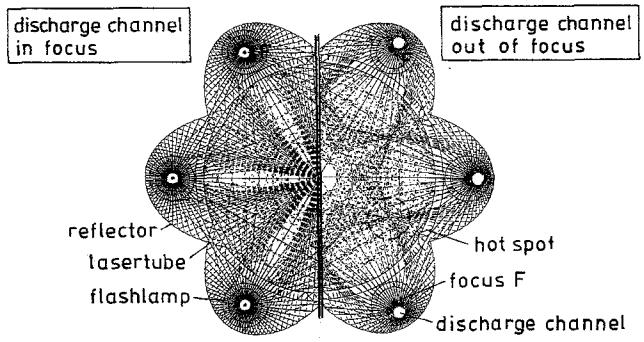

Fig. 2. Ray-tracing plot of the 5th amplifier, *Left section*: Flashlamp discharge channels and reflector focus position coincide. *Right section*: Discharge channels out of focus

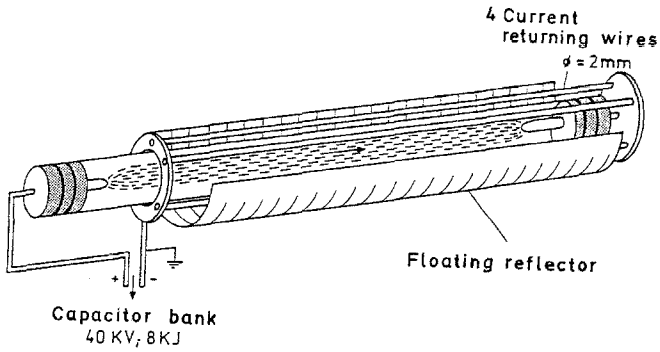

Fig. 3. Current circuit of an Asterix flashlamp

2.5 Beam-quality optimization

For an estimation of the transverse intensity and energy density profiles and wave front deformations to be expected in the Asterix IV amplifier chain the 3-D-pulse propagation code ISTERN has been developed [12]. In this program saturation, diffraction, and gas dynamic effects, which lead to refractive index gradients, are included. The computations are based on a numerical solution of the paraxial wave equation employing the fast-Fourier-transform algorithm. When the input pulse, the radial and azimuthal profiles of the inversion in the amplifiers, their apertures and positions within the chain and the specifications of the image relaying system are given, the output pulse data such as energy, pulse width, intensity and energy density profiles, and wave front deformations can be calculated. This program has also been employed as a valuable tool for optimizing the profiles of soft apertures and their positions in the chain in order to get optimal filling factors for the amplifiers and hence optimal energy output.

2.6 Damage-threshold enhancement of optical components

Thin film polarizers and anti-reflective coatings are the optical components most sensitive to laser induced

damage. The failure of coated transmission optics has several causes. The most serious one is absorption of laser energy in particles trapped in the glass/coating interface. Others being differences in thermal expansion properties between coating and substrate, which may lead to internal stresses and rupture when suddenly heated by short laser pulses, and coating inhomogeneities, particularly in large optics.

2.6.1 Anti-reflective layers. An alternative to thin film anti-reflection coatings is the Neutral Solution Process (NSP), a method originally developed by Schröder [13] and later refined by Schott [14]. This is a surface treatment with controlled corrosion in nearly neutral solution. It is applicable to borosilicate glasses such as BK7, which is exclusively used in the Asterix facility. In spring 1991, MPQ acquired a license for the NSP from Schott. We applied the NSP to the fundamental wavelength (1315 nm) and the third harmonic (438 nm) of the iodine laser and improved the production technique as well as the reproducibility and the reliability of the process in many respects [15]. Components of up to 400 mm in diameter were successfully treated by us.

Figure 4 shows the transmission spectrum of a 7 mm thick sample. It is produced as a hybrid to be used at 1 ω (1315 nm) and 3 ω (438 nm). Since the transmission had to be optimized for two different wavelengths with preference for the fundamental one, the highest possible transmission value of 99.9% achievable by the NSP when maximized for 1315 nm only could not be realized. However, the actual difference is rather small and only amounts to 0.4%. In contrast to this the difference at 438 nm between the ideal value of 100% and the actual value is 1.8%. This result is a typical behaviour of samples treated by NSP. At present, there seems to be no way to improve the transmission at 3 ω significantly. Even if the transmission is optimized for 3 ω, no higher values than 98.5% are obtainable as can be concluded from the second maximum at 460 nm. The layer is obviously too thin and the characteristics of the alkali depletion zone and the built-on aluminosilicates are not developed enough to provide a full anti-reflective effect. Not before a wavelength of about 700 nm are the transmission maxima close to 100%.

We carried out a lot of damage threshold measurements of NSP treated samples [15]. We found a value of 25 J/cm^2 for 1 shot on 1 site (1-on-1). This is about 2.5 the value for electron-gun deposited anti-reflective coatings, measured under the same conditions. Measurements with many shots of equal energy on 1 site (s-on-1) at a fluence of 70 to 80% of the 1-on-1 damage threshold showed no damage at all after more than 20 shots what is in marked contrast to the commonly used TiO_2/SiO_2 anti-reflective coatings. Since the surfaces treated by the NSP also proved to be insensitive to alkyliodide and moisture covering–both mechanisms could increase the reflectivity–we decided to treat all Asterix windows and beam splitters loaded with high fluences as well as the associated target chamber optics by the NSP.

An alternative to the NSP is the sol-gel technique also developed by Schott and later refined at Livemore/USA and at Centre d'Etudes de Limeil Velenton (CEL-V)/France [16, 17]. It is not based on corrosion but consists in depositing uniform layers of oxide based colloidal suspensions on substrates such as glass, quartz, or frequency conversion crystals. Not only anti-reflective coatings but also high-reflectivity and polarizing coatings can be fabricated. The diameter of the substrates may vary from 1 to 80 cm. The layer deposition is achieved either by the well-known dipping or spinning processes or by the laminar flow coating process. The latter is a relatively new method recently developed at CEL-V.

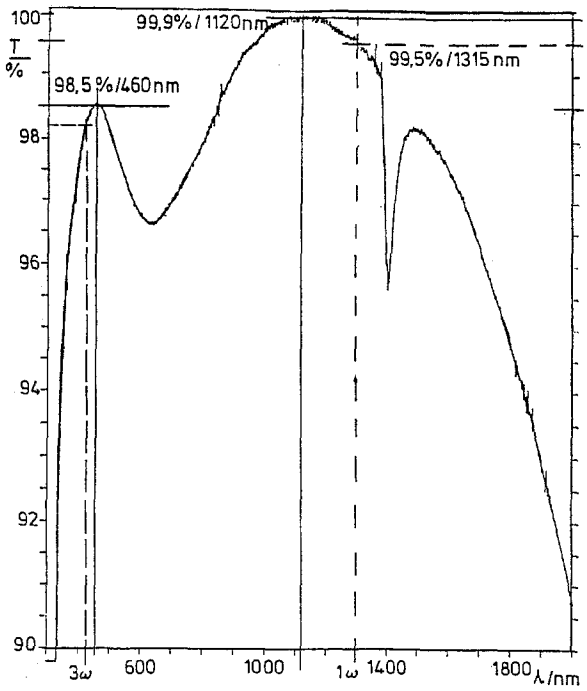

Fig. 4. The transmission is shown in the range of 90 to 100% for a sample of 7 mm thickness produced as hybrid to be used at 1 ω (1315 nm) and 3 ω (438 nm)

In the case of standard anti-reflective sol-gel coatings only a monolayer is deposited on the substrate applying usually either the spinning or the dipping process. The deposited layer consists of spherical particles of amorphous SiO_2 about 20 nm in diameter packed in a roughly 50% porous structure yielding a refractive index of 1.22 to 1.25. The spectral transmission of sol-gel monolayers is similar to that of NSP layers since both have a thickness of $\lambda/4$. Once a sample is coated with a silica layer of appropriate thickness there are no means to change its properties afterwards. When the layer turns out to be unsatisfying it can be wiped off. After that a new layer can be put on. According to our measurements sol-gel layers deposited on BK7 substrates at CEL-V/France reach damage thresholds of 19 J/cm^2 (1-on-1) and 29 J/cm^2 for 0.6 ns/1315 nm pulses if the same site is exposed to multiple shots with large increments in the fluences from shot to shot (n-on-1). These values are comparable to those obtained for NSP layers.

Whereas NSP requires a temperature of 87°C the sol-gel technique only needs room temperature. This is advantageous for stressed samples which may not tolerate

temperatures much above room temperature. This is, e.g., the case for our target lens which bears internal stresses due to a hole drilled in the region around the axis in order to avoid optical damage resulting from internal reflections which concentrate on axis. This lens was covered with a sol-gel layer at CEL-V to minimize its transmission losses. We also checked a sol-gel anti-reflective layer on two windows of the fifth amplifier (21 cm diameter). In both cases we found an excellent performance: no damage and no loss in transmission so far.

2.6.2 Polarizers. In almost any amplifier chain the polarizers belong to the optically weakest components. Our polarizers were no exceptions in this respect. The first we used had multilayer TiO_2/SiO_2 films. Their original damage threshold (1-on-1) was 8 J/cm^2, but decreased from shot to shot and finally stabilized at 1 J/cm^2. We then switched to HfO_2/SiO_2 films with an original damage threshold of 4 J/cm^2. By applying the method of laser conditioning or laser annealing [18]–that is, the layer system is "hardened" by exposing it to a series of pulses with incrementally higher and higher fluences beginning at a fluence of about one third of the single-shot damage threshold–we could raise the damage threshold significantly. We found a permanently improved value of 8 J/cm^2 for 1315 nm pulses of 0.6 ns duration. Arguments to understand this increase and its underlying mechanisms are given in [19].

The sol-gel technique can also be applied to the generation of multilayer thin film polarizers. In this case layers with low and high refractive indices are deposited on the substrate in an alternating manner. The low-refractive index layer is based on SiO_2, the high-refractive index layer either on ZrO_2 or HfO_2 instead of the commonly used TiO_2 [17]. An interesting modification of this technique is the production of low-cost polarizers coated simultaneously on each side of a BK7 or quartz glass substrate with only two layers, SiO_2 and either ZrO_2 or HfO_2-[20]. In order to achieve a constant ratio of about 250:1 calculations show that these polarizers have to be inclined at an angle of incidence of 70 to 72° instead of the Brewster angle of 56°. In addition, a stack of 3 plates in necessary. Preliminary tests with a two-layer polarizer which was sol-gel coated with SiO_2/ZrO_2 on both sides for 1315 nm confirmed the theoretical predictions. The measured contrast ratio was 12 and the transmission for p-polarized light reached a value of 97%. The 1-on-1 damage threshold of 8 J/cm^2 at a pulse duration of 0.5 ns could be slightly raised to 9 J/cm^2 by laser conditioning. These results are in fair agreement with previous experiments at 1054 nm (Priv. Commun. by Floch, CEL-V). These low-cost polarizers are especially attractive for multi-beamlets laser systems with output energies in the MJ range where hundreds of polarizers may be needed to guarantee a definite polarization state of the pulses entering the frequency conversion crystals.

3 Laser performance

Since November 1988 the Asterix IV laser is in use for laser-plasma- and X-ray laser experiments. According to the experimental needs about 1000 target shots are delivered within a year. The laser achieves a maximum output energy of 2.1 kJ at a pulse length of 5 ns, presently generated by the long-pulse oscillator. The maximum power is 3 TW obtained at $t_p = 0.4$ ns, the shortest pulse length until now employed for target experiments. Thus, the projected performance concerning output energy and power was readily achieved. For long pulses ($t_p > 1$ ns) the laser performance is limited by the available pumping energy, for pulses of medium duration ($t_p = 0.3$–1 ns) by optical damage and for short pulses ($t_p < 0.3$ ns) by small-scale self-focusing.

The obtained pulse data are in good agreement with the values computed by both codes and they also correspond to the projected overall efficiency of $\eta = 0.16\%$ twice as much as that of the previous system Asterix III. The laser light has been converted into the second harmonic with an efficiency of over 60% and into the third harmonic with an efficiency of 56% (with the inclusion of all losses). Behind the 6th amplifier the focusability was measured to be better than 4 times diffraction limited both at 1 ω and 3 ω. The 1-ω energy density distribution recorded in a plane equivalent to that of the frequency conversion crystals shows a smooth and nearly rectangular profile with a relative maximum deviation from the mean value of at most $\pm$ 6% (Fig. 5). The profiles at 3 ω are equally good.

The laser shows a very dependable and stable performance. Its reliability defined as perfect shots over delivered shots has been found to be better than 95% for a typical target shot period of 400 shots. Also the output energy is very constant during this period. Its relative standard deviation from the mean value is $\pm$ 4% and in short term use (12 shots) $\pm$ 1.3%. The directional stability of the laser beam during a shot sequence is $< \pm$ 50 µrad and thus satisfies all requirements. The laser also does not need any beam realignment within months. Because of these facts, its moderate maintenance effort, and the high shot rate (1 shot/20 min), the Asterix IV laser has been proven to be a very valuable tool for laser-plasma- and X-ray laser experiments.

4 Scalability and prospects

The flash lamp-pumped iodine laser has the potential to be scaled up to still higher output energies and powers than those achieved in Asterix IV. Amplifiers with diameters in the 1m range can be realized. Calculations based on the experience gained with the Asterix IV laser predict an output energy of 10 kJ for an end amplifier with an aperture of 70 cm.

An iodine laser system can be considerably simplified if the final high-power amplifier is double passed using a value of 200 up to 1000 for the one-way small signal amplification A_{SS}. Under these conditions only a rather low input energy is needed to get access to a fraction of the stored energy which is not as high as that obtainable with the system described above but still has a reasonable value. This and the strongly reduced system complexity makes the "lean configuration" an attractive option. The basic reason for the favorable energy extraction behaviour

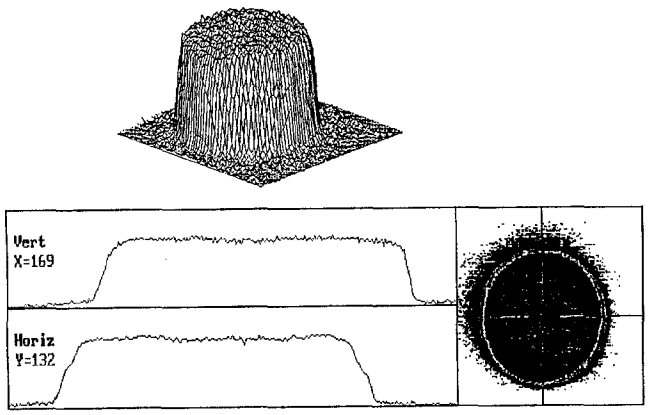

Fig. 5. Vidicon record at 1 ω of a typical energy density profile in a plane equivalent to that of the frequency conversion crystals (background noise not subtracted)

is the low value of the saturation energy density of only ≈ 0.9 J/cm^2. (The corresponding value in glass is 5 J/cm^2 requiring thus many passes instead of only two to achieve a satisfying energy extraction.)

To avoid parastic oscillations in the amplifier the two passes must be optically decoupled. One possibility is to use a phase conjugating mirror based on stimulated Brillouin backscattering (SBS). This mirror offers reflectivities between 60 and 70% for relatively modest input energies. It is active during the interaction time pluse the phonon decay time what in the case of SF_6 as the most appropriate SBS medium for the iodine laser amounts alltogether to a coupling period of ≈ 100 ns. Moreover, the SBS process may also be used for pulse shortening and – by virtue of its phase conjugating nature – simultaneously for the correction of wave front distortions caused by pump-light-induced refractive index inhomogeneities. This concept was successfully tested by Bessarab et al. [21] in a chain consisting of two amplifiers of 120 cm diameter and a length of 4 and 5 m, respectively. At an A_{SS} value in excess of 1000 an input energy of only 6 mJ was sufficient to achieve an output energy of 6 kJ. The amplified pulse when returning from the SBS mirror and impinging again on the mirror serving for the coupling of the input pulse to the amplifier makes this element highly transparent by a sudden evaporation of the high-reflectivity bismut coating. This so-called clarifying mirror thus only holds for one shot.

This serious disadvantage being rather inconvenient for multiple pulse-per-hour operation is avoided in the design schematically sketeched in Fig. 6 where the last amplifier of Asterix is used. The Brillouin mirror is replaced by an ordinary mirror. The two-pass small-signal amplification is reduced to a tolerable value by a saturable absorber with a small-signal transmission of 2%. The overall reflectivity of the combination mirror–*saturated* absorber is 50%. The direction of the back-reflected pulse is slightly different from that of the incoming so that the former does not fire back into the front-end driver. Instead, on its way to the target it passes through a second pinhole adjacent to the first pinhole which is thus only used by the incoming pulse. The shutter necessary to decouple the front-end driver from the amplifier only needs a contrast ratio of 10^6:1 which is not difficult to achieve.

Figure 7 shows the expected output energy vs input energy for a stored energy density of 5 J/cm^2 at A_{SS} values of 200 and 300. Higher values are hardly accessible since the lenses must then bear an anti-reflective coating with $R \leq 0.1\%$ which is practically difficult to achieve over long operation periods. The amplifier windows are not that critical due to their slight inclination. Beyond input energies of 200 mJ output energies in excess of 1 kJ are

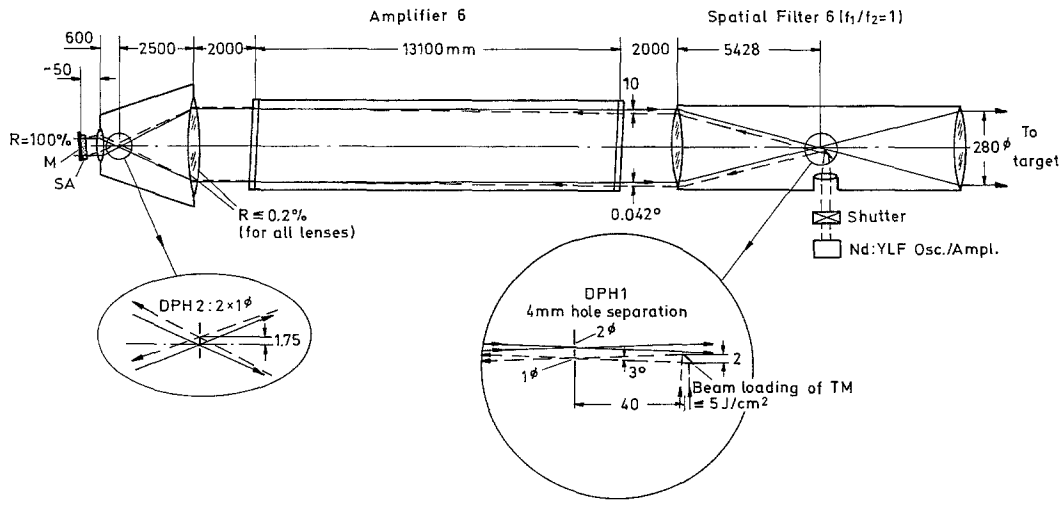

Fig. 6. Double passed Asterix amplifier A6. *M*, plane mirror with 100% reflectivity; *SA*, saturable absorber JUL II with small signal transmission $T_{SS} = 2\%$, and large signal transmission $T_{LS} = 0.75$. The shutter decouples the front-end driver, a Nd:YLF oscillator/amplifier system, from the amplifier A6. *DPH1* and *DPH2*, double pin-holes; TM: turning mirror

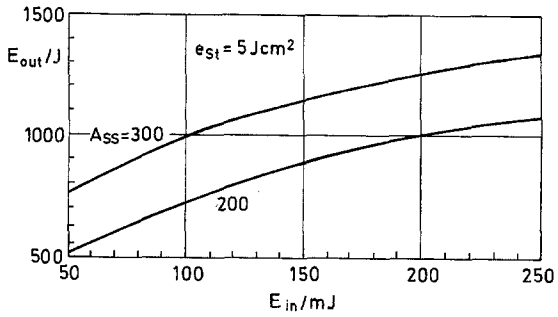

Fig. 7. Output energy of the double passed Asterix amplifier A6 vs input energy. The stored energy density e_{st} is the energy available at the moment of amplification. The single-pass small signal amplification A_{SS} has values of 200 and 300. The beam diameter used is 280 mm. The reflectivity of the combination mirror M and saturated absorber SA is 50%

obtainable. An attractive choice for the front-end driver is a Q switched Nd:YLF oscillator/amplifier system tuned to the iodine transition and capable of delivering pulses with durations of a few up to about 20 ns. Saturation effects in the iodine amplifier and in the absorber shorten the output pulse duration to values ranging from about 1 to several ns. Due to its repetition rate of 1 Hz or more the Nd:YLF laser is also very advantageous for system and target alignment.

The iodine laser is limited towards shorter pulses by its narrow bandwidth but, nevertheless, it has the potential to be avaluable tool for the generation of multi-TW fs-pulses. Since its third harmonic (438 nm) falls within the absorption bandwidth of Ti:S crystals (400–600 nm) iodine laser pulses with durations in the ns respectively sub-ns region can be used as a pumping source for Ti:S amplifiers. First measurements of this process yielded amplification factors high enough for an application at reasonable values of the pump energy density. Computations carried out on the basis of the experimental results revealed that a 100 mJ/150 fs Ti:S laser pulse can be amplified to the 700 TW level by three double-passed amplifiers of 30, 50, and 85 mm diameter pumped at 438 nm by pulses of 0.3 ns duration with energies of 60, 90, and 200 J, respectively. This concept can, in principle, be realized with the Asterix IV iodine laser.

Acknowledgement. This work was supported in part by the Commission of the European Communities in the framework of the Association Euratom/Max-Planck-Institute für Plasmaphysik.

References

1. K. Hohla, K.L. Kompa: Appl. Phys. Lett. **22**, 77 (1970)
2. G. Brederlow, E. Fill, K.J. Witte: *The Light-Power Iodine Laser*, Springer Ser. Opt. Sci., Vol. 34 (Berlin, Heidelberg 1983) pp. 6–13
3. G.A. Kirillov, V.M. Murogov, V.T. Punin, V.I. Shemyakin: Laser Particle Beams **8**, 827 (1990)
4. L. Laska, K. Masek, J. Krasa: Czech. J. Phys. B **37**, 601 (1987)
5. G. Brederlow, R. Brodmann, K. Eidmann, M. Nippus, R. Petsch, S. Witkowski, R. Volk, K.J. Witte: IEEE J. QE-**16**, 122 (1980)
6. T. Uchiyama, K.J. Witte: IEEE J. QE-**18**, 885 (1982)
7. E.E. Fill, W. Skrlac, K.J. Witte: Opt. Commun. **37**, 123 (1981)
8. R. Volk, S. Stähler: In Proc. Workshop on Iodine Laser and Applications, Liblice (1989) pp. 44–47
9. E. Fill: Opt. Commun. **49**, 362 (1984)
10. Ch. Schrödter: MPQ Annu. Rep. 1987 (MPI für Quantenoptik, Garching 1987) pp. 180
11. R.S. Craxton: Opt. Commun. **34**, 474 (1980)
12. J. Krug, K.J. Witte: MPQ Rep. Nr. 133 (MPI für Quantenoptik, Garching 1988)
13. H. Schröder: Glastechn. Ber. **27**, 91 (1953)
14. L.M. Cook, S. Ciolek, K.H. Mader: J. Am. Ceram, Soc. **65** (9), C-152(1982)
    L.M. Cook, A.J. Marker III, K.H. Mader, H. Bach, J. Müller: Part 1–4, Glastechn. Beri. **60** (7–11) (1987)
15. Ch. Hagedorn, H. Baumhacker: MPQ Rep. 170 (MPI für Quantenoptik, Garching 1983)
16. I.M. Thomas: Appl. Opt. **25**, 1481 (1986)
17. H.G. Floch, P.F. Bellevile: In *Prog. Int' Conf. Sol-Gel.* Vol. 2, No. 123 (Cluwer, Dordreclit 1994)
18. M.R. Kozlowski, M.C. Staggs, F. Rainer, J.H. Stathes. SPIE Proc. **1441**, 269 (1991)
19. M.R. Kozlowski, C.R. Wolfe, M.C. Staggs, J.H. Campbell: SPIE Proc. **1438**, 376 (1990)
20. H. Baumhacker, E. Fill, Ch. Schrödter: Private communication MPI für Quantenoptik, Garching
21. A.V. Bessarab, Y.V. Dolgopolov, N.V. Zhidkov, G.A. Kirillov, G.G. Kochemasov, S.M. Kulikov: Izw Akad. Nauk SSSR, Ser. Fisich. **52**, 333 (1988)
    Y.V. Dolgopolov, G.A. Kirillov, G.G. Kochemasov, S.M. Kulikov, V.M. Murugov, S.N. Pevny, S.A. Sucharev, L.I. Zykov: SPIE Proc **1412**, 267 (1991); SPIE Proc. **1980**, 23 (1992)
22. H. Baumhacker, A. Grabtchikov, K.J. Witte: Tech. Dig. 8th Laser Optics Conf., St. Petersburg, Russia June 27–July 1 (1995) Paper LSB01; Appl. Phys. B (submitted)